Journal of
Computational and Theoretical Nanoscience
Vol. 8, 972–982, 2011

Signal Energy in Quantum-Dot Cellular Automata Bit Packets

Enrique Pacis Blair[1], Mo Liu[2], and Craig S. Lent[2,*]

[1] *United States Naval Academy*
[2] *University of Notre Dame*

Quantum-dot cellular automata is a novel paradigm for computing at the nanoscale. Cells are the basic computing element in quantum-dot cellular automata and function as structured charge containers rather than as current switches. Computing with quantum-dot cellular automata is enabled by quantum-mechanical tunneling and Coulomb interactions. The use of molecules as cells to realize quantum-dot cellular automata may make possible nanometer-scale devices and ultra-high device densities without excessive heat dissipation. Molecular quantum-dot cellular automata can be clocked using an external electric field. A time-varying clock can be used to drive data flow through layouts of cells. Together, the clock and the device layout define a computational architecture where data flows through the circuitry in the form of bit packets. Here we analyze the energetics of QCA bit packets. We find a heuristic model based on cell-cell interactions works well. Bit packet energies in general scale with the packet length. It may, however, be possible to design a cell geometry so that the energy is packet-length independent. Fan-out and fan-in can be understood as investing energy from the clock in the signal, and then returning the energy back to the clock.

Keywords: Molecular, Quantum-Dot Cellular Automata, QCA, Bit Packet, Cost, Fan-Out, Molecular Electronics, Recoverable Energy.

RESEARCH ARTICLE

1. INTRODUCTION

1.1. Quantum-Dot Cellular Automata

The quantum-dot cellular automata (QCA) paradigm is a novel approach to computing at the nanoscale[1,2] which is enabled by quantum-mechanical tunneling and Coulomb interactions but does not rely on the flow of current.[3] Bits are encoded in the charge configuration of cells composed of quantum dots. QCA devices can be clocked using an external electric field.[4] A time-varying clock can be used to drive data flow through arrays of cells. Together, the clock and the device layout define the circuit and computational architecture in the QCA paradigm.[5]

Linear arrays of QCA cells form binary wires through which bit packets move, not ballistically, but under clocked control. Computation occurs when bits collide in cells arranged to form logic gates. Here our focus is on the energetics of QCA bit packets themselves. We calculate the energy required to form bit packets using two methods: (a) a heuristic approach based on the pair-wise interaction of cells and characterized by several basic interaction energies, and (b) a direct Coulomb calculation that sums the interactions between charges in the system. The agreement between these two approaches justifies the use of the heuristic model. In general bit packet energy scales with the length of the packet, but we find that cells can be designed such that the signal energy is constant with respect to the packet length. The signal energy cost is paid just at the "surfaces" of the bit packet. We examine the energetics of fan-out and fan-in. We find that again the notion of a packet energy is useful: the energetic cost of replicating a bit through fan-out is just the cost of creating new bit packets. That energy is returned to the clock in a fan-in.

It is important to note that QCA is not quantum computing. Though quantum mechanics provides the all-important "grease" of tunneling that makes switching possible, information is encoded in classical degrees of freedom—the quadrupole moment of the cell charge configuration—not in the coefficients of a quantum mechanical superposition state. This makes computation more robust, though limited to conventional bits rather than q-bits. QCA is aimed at general-purpose computing.

1.2. QCA Implementations

Functioning QCA cells and assemblies of cells forming more complex circuits have been synthesized by the

*Author to whom correspondence should be addressed.

 1546-1955/2011/8/972/011 doi:10.1166/jctn.2011.1777

Notre Dame group.[6–24] In these experiments aluminum islands act as the dots, coupled by aluminum oxide tunnel junctions. The islands and junctions are formed by e-beam lithography and two angled metal evaporations with an intervening oxidation step. Overlaps between the two metal layers create the tunnel junctions. Because the shadow evaporation technique produces capacitances that are still relatively large, these experiments are performed at cryogenic temperatures (<1 K).

Using these metal-dot QCA cells and number of important circuit elements have been demonstrated: functioning individual cells,[6] logic gates,[14] clocked QCA cells,[16, 23] inverters,[22] memories,[18] and shift registers.[20] In addition power gain greater than 3 has been measured.[25] Power gain is important so that small energy losses due to inevitable inelastic processes can be restored. In QCA the energy lost to dissipative processes is restored from the clock. Fan-out of QCA signals has also been demonstrated experimentally.[26]

In addition to the metal-dot QCA work at Notre Dame, other groups have succeeded in building QCA cells in semiconductors. Mitic et al. reported fabrication of QCA cells in silicon using dots formed by few-atom implantation of phosphorus donors.[27] Perez-Martinez et al. created QCA cells using gate-defined dots in a GaAs two-dimensional electron gas.[28] As with the metal dot systems, lithographically defined dots, whether in silicon or GaAs, are relatively large so that the Coulomb energies involved are small and operating QCA cells can only function at cryogenic temperatures. QCA can also be implemented in magnetic systems comprised of small permalloy islands.[29, 30]

The Wolkow group at the University of Alberta recently fabricated a QCA cell using single-atom dangling bonds on a H-passivated Si surface as the quantum dots.[31] Individual hydrogen atoms were removed from the surface to expose the Si dangling bonds (DBs) using STM lithography. Coulombic interactions between nearby DB dots was apparent in the brightness of the STM images. By electrostatically perturbing a symmetric four-dot cell, the polarization of the QCA cell was apparent. These room temperature results confirm the viability of molecular-scale QCA. Work is underway to construct room-temperature QCA cells from molecules designed for the purpose.[32–37]

2. QCA CELLS AND DEVICES

2.1. Dots, Cells, and Logic Gates

The elementary computing device in QCA circuitry is the QCA cell,[38] a charge-containing structure with multiple sites, quantum dots, which localize mobile charges. Device switching is enabled by quantum-mechanical tunneling. A cell with two mobile charges and four dots arranged in a square has two preferred states with electrons in antipodal dots (see Fig. 1). These states are degenerate in energy and can be used to represent binary "0" and "1", respectively.

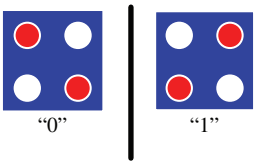

Fig. 1. The two states of a four-dot QCA cell with two mobile charges and four dots. A quantum dot is represented by a white disc, and the red disc within a white disc represents a mobile charge occupying a dot.

The basis of QCA circuitry is intercellular interaction via Coulomb repulsion. The interaction between cells lifts the degeneracy between the 0 and 1 states and determines the state of the cell. Broadside coupling causes neighboring cells to align (Fig. 2). This is the basis for the binary wire (Fig. 3).[39] Signal inversion can be achieved via diagonal coupling (Fig. 3). The majority gate is a three-input gate having a single output which is determined by the bit dominating the three inputs (Fig. 3). One of the three inputs can be used as a control input to make the majority gate function as a programmable AND-OR gate. This is seen in the truth table for the majority gate (Table I). The QCA paradigm is heirarchical, and QCA-based adders and even a Simple-12 ALU processor have been designed.[3, 38]

2.2. Clocked QCA Cells

Clocking QCA cells provides power gain for the restoration of weakened signals, minimizes power dissipation,[25, 40] and facilitates large-scale circuit operation.[41] QCA cells can be clocked if two additional dots, called "null dots," are added and the voltage on the null dots can be controlled. The null dots add an additional state, called the "null state," which, does not convey information (the information-bearing states are now called "active states") as shown in Figure 4. The voltage of the null dots can be used to drive the cell to an active state or force the cell into the null state. A cell in the null state does not lift the degeneracy of the active states in a neighboring cell. Clocked devices such as shift registers have been demonstrated.[42]

The state of a six-dot cell can be characterized by two quantities: polarization P and activation A. The quantities P and A originate in a three-state quantum-mechanical

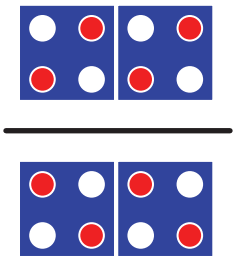

Fig. 2. Broadside coupling causes cells to align.

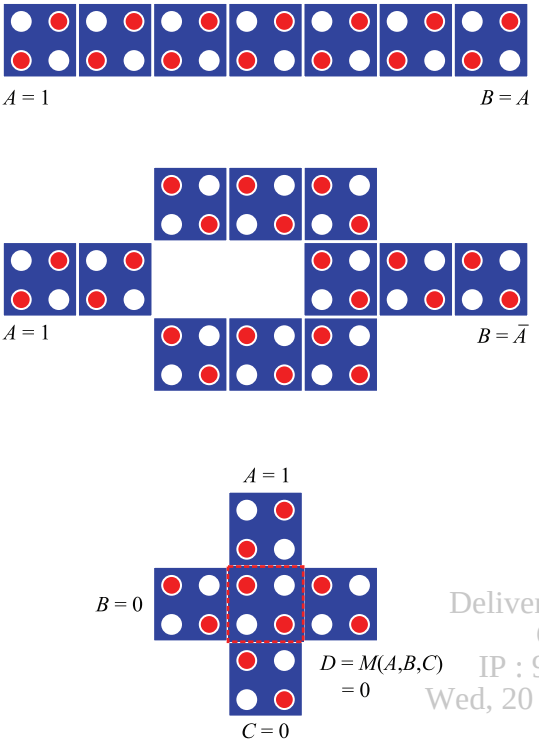

Fig. 3. Basic QCA devices: binary wire (top); inverter (middle); majority gate (bottom). The majority gate has three inputs (A, B, and C). The inputs "vote" at the device cell (in the red dashed box), and the output (D) is copied from the device cell. Here, two input zeros dominate a single one, and the output is zero.

description of a six-dot QCA cell as discussed in Appendices 7 and 7.1. P and A, respectively, are functions of the expectation values of $\boldsymbol{\lambda_7}$ and $\boldsymbol{\lambda_8}$, two of the eight generators of SU(3), sometimes called the Gell-Mann matrices (see Appendix 7.1), used in calculating the quantum dynamics of a QCA cell coupled to a dissipative heat bath.[43] P and A are defined by

$$P = -\langle \boldsymbol{\lambda_7} \rangle \tag{1}$$

$$A = \frac{2 - \sqrt{3}\langle \boldsymbol{\lambda_8} \rangle}{4} \tag{2}$$

Table I. The truth table for a MAJORITY gate is partitioned to highlight the ability of MAJORITY gates to function as programmable two-input AND-OR gates. Let A be the control input. If $A = 0$, then $D = BC$; if $A = 1$, then $D = B + C$.

A	B	C	$D = M(A, B, C)$
0	0	0	0
0	0	1	0
0	1	0	0
0	1	1	1
1	0	0	0
1	0	1	1
1	1	0	1
1	1	1	1

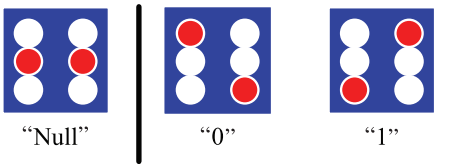

Fig. 4. Three states of a six-dot cell.

The polarization and activity can also can be expressed more directly as functions of the charge on the dots of a QCA cell. With dots numbered as in Figure 5, P and A are:

$$P = q_1 + q_4 - (q_3 + q_6)/Q \tag{3}$$

$$A = 1 - (q_2 + q_5)/Q \tag{4}$$

where q_i is the charge on the ith dot and $Q = \sum q_i$. These expressions are valid regardless of the sign of the mobile charge. A ranges from 0 to 1; P ranges from -1 to 1 and must satisfy $|P| \leq A$. A fully active cell has $A = 1$. A cell in the null state has $(P, A) = (0, 0)$. A fully active, completely polarized cell has $(P, A) = (1, 1)$ (corresponding to the "1" bit) or $(P, A) = (-1, 1)$ (corresponding to the "0" bit).

2.3. Clocking Molecular QCA Cells

Molecular QCA allow room-temperature operation. Fixed charge in a molecular QCA cell (ligand charges) can balance the mobile charge to give the molecule a net zero charge. Numerous possibilities exist for the configuration and placement of neutralizing charge and add to the design space for QCA cells.[36, 44, 45]

Clocked molecular QCA cells can be designed with coplanar active dots and null dots which lie outside of this plane. Such molecules can be clocked without individual electrical connections to each cell, but rather using the vertical component of an electric field[4] as shown in Figure 6. Such an electric field can be created using an array of wires buried in the substrate below the device plane on which the QCA devices lie. A multi-phase clock signal can be applied to the conductors yielding regions of the device plane where cells are active and other regions are null, as depicted in Figure 7. Moreover, the time-varying nature of the clock will cause "active domains" to flow through the QCA circuitry in a controlled manner. As active domains move throughout the circuitry, they carry

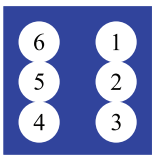

Fig. 5. A six-dot cell with dots numbered for reference.

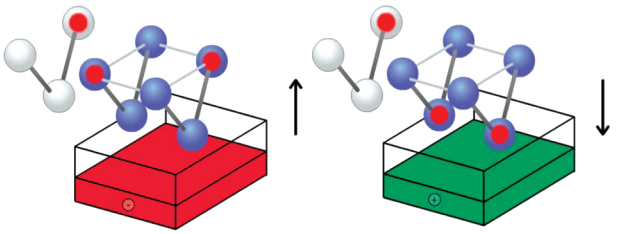

Fig. 6. A six-dot cell can be clocked using a conductor buried below the substrate. Here, a cell's six dots are represented by blue spheres; mobile charges—in this case, two electrons—are represented by red circles. When the conductor is negatively charged (left, conductor colored red), it creates an electric field that drives the mobile charge upward, and the cell takes an active state. When positively charged (right, conductor shown in green), the conductor's electric field draws the electrons down to the null dots, and the cell takes the null state.

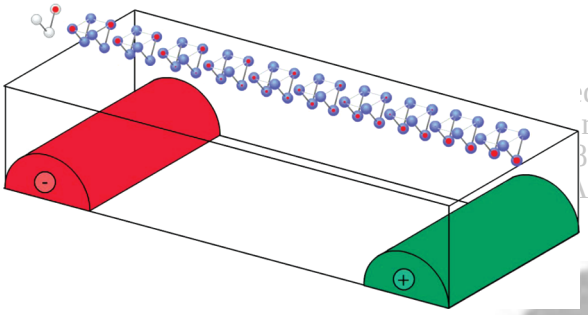

Fig. 7. Charged clocking wires activate some molecular QCA cells on the substrate while driving other cells to the null state, thus forming active and null domains.

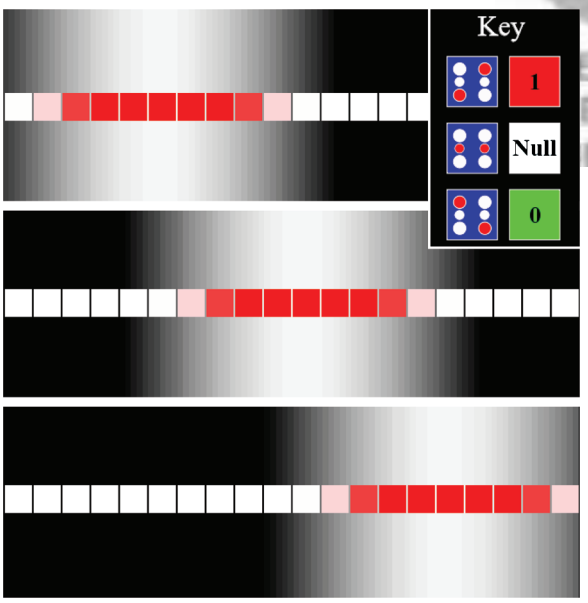

Fig. 8. A moving active domain pushes a bit packet (in this case, a "1") rightward through a binary wire. The color of the background represents the vertical component of the electrical field. The white region is the moving active domain, and the black region is the null domain. Three snapshots in time are shown arranged early to late from top to bottom.

signals in the form of bit packets as in Figure 8. Null domains are regions where cells are not active, and the frontier between the null domains and active domains is a transition region in which computation occurs.[5]

3. THE ENERGETICS OF QCA BIT PACKETS

3.1. Interactions Between Neighboring Cells

An expression for the cost of a bit packet can be developed by accounting for changes in the basic intercellular interactions present. The states of interest in an isolated cell are illustrated in Figure 9. The active states $(P, A) = (\pm 1, 1)$ are degenerate, and the energy E_{c0} of the null state $[(P, A) = (0, 0)]$ is driven by the clock bias.

For a cell with a single neighbor in the null state (depicted in Fig. 10), the active states remain degenerate, although they both may be raised by E_{hn1}, the energy of broadside interaction between a polarized cell and a null cell. The null state energy will be raised by E_{hnn}, the energy of electrostatic broadside interaction between two null cells. In Figure 10, E_{hn1} and E_{hnn} arbitrarily are depicted as having negative and positive values, respectively; but this need not be the case.

When a cell has broadside coupling with a single neighbor in a fully polarized state, as in Figure 11, the degeneracy in the cell's active-state energy levels is lifted. The cell's preferred (ground) state matches its neighbor's state. The preferred state's energy shifts by an amount E_h, the horizontal broadside coupling energy between aligned active cells. The non-preferred active state shifts by an amount $E_h + E_k$, where E_k is identified as the kink energy. E_k is the cost of having two adjacent cells in opposing states relative to the energy of the same cells in an aligned configuration. The cell's null state is raised by E_{hn1} (in this case, $E_{hn1} < 0$ for consistency with Fig. 10).

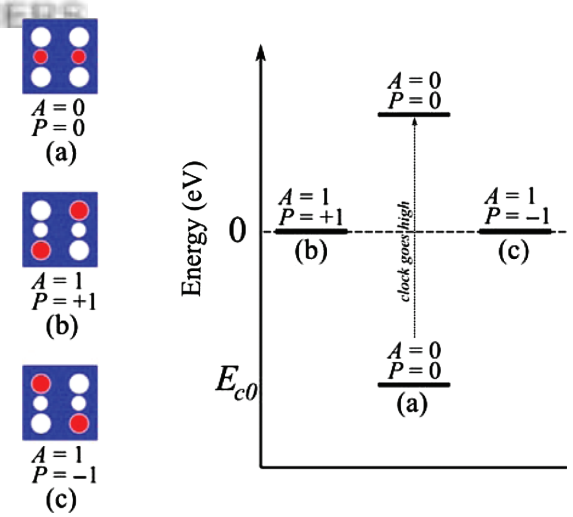

Fig. 9. Energy levels for an isolated QCA cell. In this figure and subsequent figures, the null dots are drawn smaller than the active dots to indicate that they are on a plane below that of the active dots.

RESEARCH ARTICLE

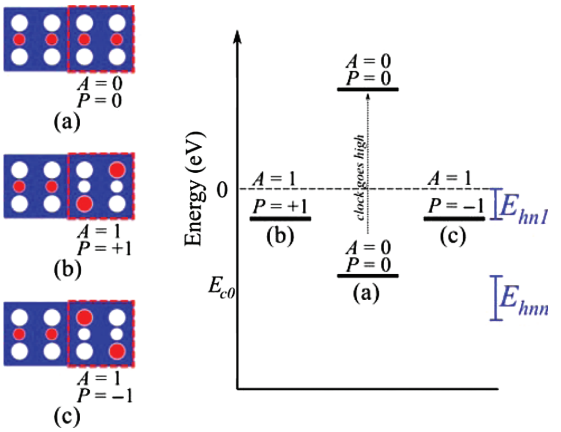

Fig. 10. Energy levels for a QCA cell having a single neighbor in the null state. The neighboring cell's null state does not lift the degeneracy of the active states, but it raises the null state of the active cell (identified with a red dashed box) by the horizontal null-null energy E_{hnn} (here, E_{hnn} arbitrarily is shown as positive and E_{hn1} is shown as negative).

3.2. The Energy of a Bit Packet of Length N

3.2.1. The Reference State

The energy cost of a bit packet will be referenced to the energy E_{ref} of a wire with all cells in the null state. Thus, it is helpful to understand the interactions present in such a wire. Consider only interactions between adjacent cells (nearest-neighbor interactions) in a L-cell wire. Each cell in the null state with no additional clock contributes $-E_{\text{c0}}$ to the system cost, and each of the $L-1$ nearest-neighbor null-null interactions raise the system energy by E_{hnn} so that the reference energy of the wire is

$$E_{\text{ref}} = -LE_{\text{c0}} + (L-1)E_{\text{hnn}} \tag{5}$$

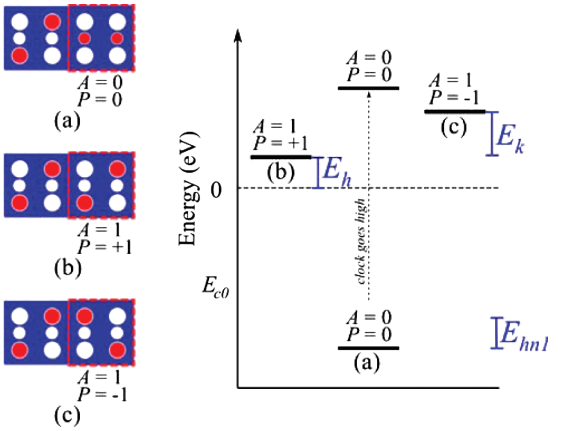

Fig. 11. Energy levels for a QCA cell having a single polarized neighbor. The polarized neighbor lifts the degeneracy of the cell's active states, and the null-state energy is shifted up by the energy E_{hn1} of interaction between a null cell and a polarized cell (in this case, $E_{\text{hn1}} < 0$ for consistency with Fig. 10).

3.2.2. Heuristic Model

We first construct a model of the energy of a bit packed by summing the various relevant interaction. The advantage of this heuristic approach is it's generality. It is appropriate for many types of QCA implementations, including metal-dot, molecular, and even magnetic, because the model is derived from cell-cell interaction energies. Since our focus here is on clocked molecular QCA, we validate the model by direct summation of the Coulomb energies.

Consider activating a bit packet N cells long anywhere along the wire of length L cells except at the edges. To activate the first cell in the array costs E_{c0}; however, two horizontal null-null interactions each are replaced by an interaction between a null cell and a polarized cell of energy E_{hn1}. The total cost E of activating the first cell in the bit packet is

$$E = E_{\text{c0}} - 2E_{\text{hnn}} + 2E_{\text{hn1}} \tag{6}$$

Each of the $N-1$ subsequent cells activated in the N-cell packet costs an additional E_{c0}, saves another E_{hnn}, and introduces E_{h}, the interaction energy between two aligned, fully active cells. One of the previously-introduced interactions having an energy of E_{hn1} is removed but is reestablished at the new end of the bit packet. The total cost E of the N-cell bit packet ($N \geq 1$) is

$$E = NE_{\text{c0}} - (N+1)E_{\text{hnn}} + (N-1)E_{\text{h}} + 2E_{\text{hn1}} \tag{7}$$

E_{hnn}, E_{nh1}, E_{h}, and various other interactions with their corresponding energy value are illustrated and cataloged in Figure 12.

3.2.3. Direct Coulomb Model

Figure 13 shows that packet costs predicted using Eq. (7) match values calculated by considering all the pairwise Coulombic energies in the system. Calculated packet costs were determined by summing the energy input from the clock and the electrostatic potential developed by nearest-neighbor and next-nearest-neighbor intercellular interactions as follows:

$$E_{\text{calculated}} = \sum_{j=1}^{m} q_{j,\,\text{null}} V_{j,\,\text{clock}} + \sum_{j=1}^{m} \sum_{i=1}^{s_j} q_{j,\,i} V_{j,\,i,\,\text{neighbors}} \tag{8}$$

where m is the number of cells in the system. $q_{j,\,\text{null}}$ is the charge on the null dots of the jth cell; $V_{j,\,\text{clock}}$ is the electrostatic potential at the null dots of the jth cell due to the clock. $V_{j,\,\text{clock}}$ is the sum of two components: a bias V_{c0} and an additional variable voltage value V_{c} used to activate or deactivate cells. For calculating intercellular interactions, the jth cell is represented by s_j point charges in space, of which $q_{j,\,i}$ is the ith. $q_{j,\,i}$ is either a mobile charge occupying one of the six quantum dots of the jth cell or a neutralizing charge at a fixed location within the jth cell.

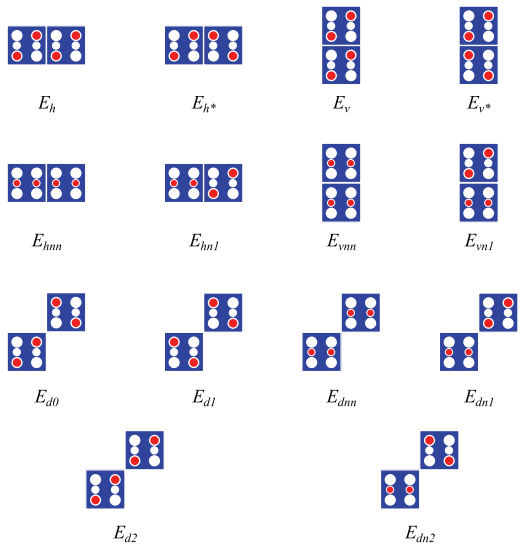

Fig. 12. Basic nearest-neighbor broadside and next-nearest-neighbor diagonal QCA interactions and associated energy identifiers are cataloged and illustrated. For each energy given, degenerate states are not shown. The subscripts h, v, and d indicate horizontal broadside coupling, vertical broadside coupling, and diagonal coupling, respectively. The number of "n"s occurring in a subscript indicate the number of cells in the interaction that are in the null state. Numbers and stars appearing in the subscript differentiate between similar interactions.

$V_{j,i,\text{neighbors}}$ is the electrostatic potential at the location of each charge $q_{j,i}$ of the jth cell due the charges comprising cells which are neighbors to the jth cell. To avoid double-counting neighbor interactions, all cells are given a numeric index, and only those nearest or next-nearest neighbors having an index k such that $k > j$ contribute to $V_{j,i,\text{neighbors}}$. $V_{j,i,\text{neighbors}}$ is calculated

$$V_{j,i,\text{neighbors}} = \frac{1}{4\pi\epsilon_0} \sum_{k=j+1}^{m} \sum_{p=1}^{s_k} \frac{q_{k,p}}{r_{i,p}} \tag{9}$$

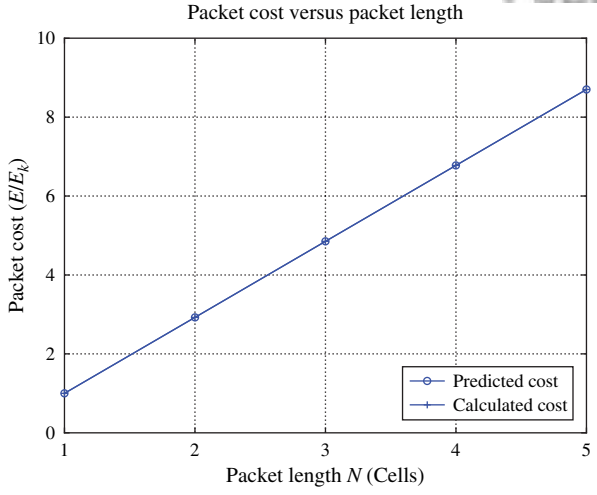

Fig. 13. The cost of a bit packet of length N predicted using (7) agrees with values calculated from the direct Coulomb model. Energies are given in multiples of the kink energy E_k.

where $q_{k,p}$ is the pth point charge—fixed or mobile—of the kth cell; a total of s_k charges comprise the kth cell; $r_{i,p}$ is the distance between $q_{j,i}$ and $q_{k,p}$; the entire array of cells in consideration has a total of m cells; and, ϵ_0 is the permittivity of free space.

Figure 14 illustrates the cell geometry. The origin is taken to be a point on the substrate at the center of the cell. The active dots form an a-by-a square centered above the origin, and they lie in a plane that is z_{act} above the null dots. The null dots are assumed to be on the line $y = 0$ at a height of $z = 0$, and each lies a distance x_{null} from the origin. For the predicted and calculated packet costs reported in Figure 13, cells having $(a, x_{\text{null}}, z_{\text{act}}) = (0.7, 0.35, 0.35)$ nm were used; and one positive (neutralizing) elementary charge is located at each null dot. Cells were spaced such that adjacent cells with broadside coupling have a center-to-center spacing of $2a$. The clock bias V_{c0} was set such that the energy E_{c0} of an isolated cell's null state is $E_{\text{c0}} = -E_k$.

3.3. Design of Constant-Energy Bit Packets

Equation (7) may be written:

$$E = N(E_{\text{c0}} - E_{\text{hnn}} + E_{\text{h}}) - (E_{\text{hnn}} + E_{\text{h}} - 2E_{\text{hn1}}) \tag{10}$$

The design space for QCA cells can be used to achieve particular behaviors. We can choose E_{c0} and cell geometry so that $E_{\text{h}} = -E_{\text{c0}} + E_{\text{hnn}}$. This removes the length-dependence from the cost E of a bit packet, reducing the cost to a constant: $E = -(E_{\text{hnn}} + E_{\text{h}} - 2E_{\text{hn1}})$. This constant $-(E_{\text{hnn}} + E_{\text{h}} - 2E_{\text{hn1}})$ may be understood as the surface area cost of having the interface at either end of the bit packet, each costing $-(E_{\text{hnn}} + E_{\text{h}} - 2E_{\text{hn1}})/2$. A specific cell design that exhibits this length independence has $(a, x_{\text{null}}, z_{\text{act}}) = (0.7, 0.175, 0.0875)$ nm (reasonable molecular dimensions). Its length-independent packet cost is seen in Figure 15. For this design, one positive elementary half-charge is fixed at each active dot, crudely

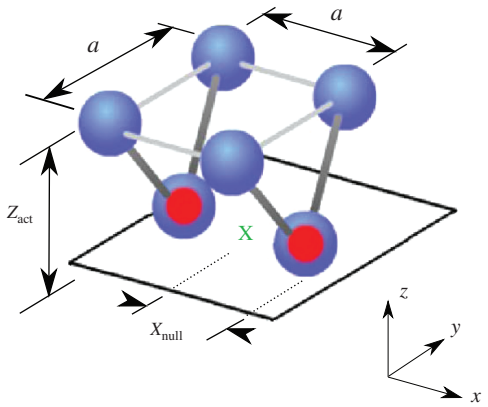

Fig. 14. The geometry of a QCA cell. The origin, indicated by a green "x," is taken to be in the plane of the lower dots at the cell center.

RESEARCH ARTICLE

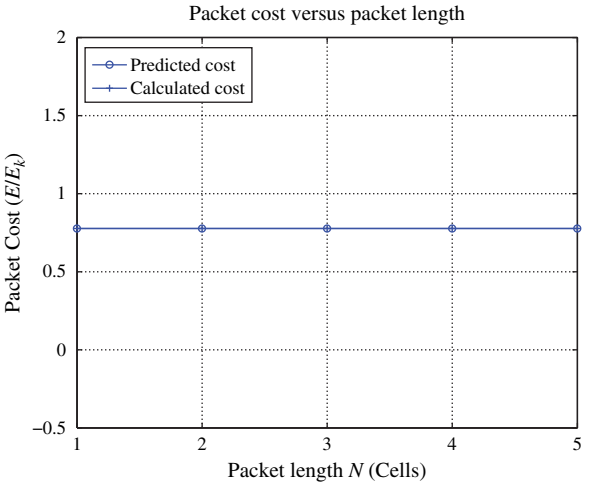

Fig. 15. QCA cells can be designed to have an energy cost independent of the length of the bit-packet. The energy cost is shown as predicted by the heuristic model and calculated by the direct Coulomb model.

approximating a possible neutral molecule. A center-to-center spacing of 1.4 nm was used for adjacent cells having horizontal coupling. The clock bias V_{c0} was set such that $E_{c0} = -0.673E_k$.

4. THE ENERGETICS OF FAN-OUT AND FAN-IN

QCA fan-out is the branching of a single bit packet into two identical packets as it is pushed along a wire which branches into two wires. This is accomplished using a fan-out circuit depicted in Figure 16. The additional cost of fan-out is the cost of the second packet, which is equal to the cost of the first packet (Fig. 17).

A bit packet can be fanned out into two packets and then fanned in back to one using a circuit as shown in Figure 18. Work equal to the cost of replicating the original bit packet is done on the clock when fan-in occurs (Fig. 19).

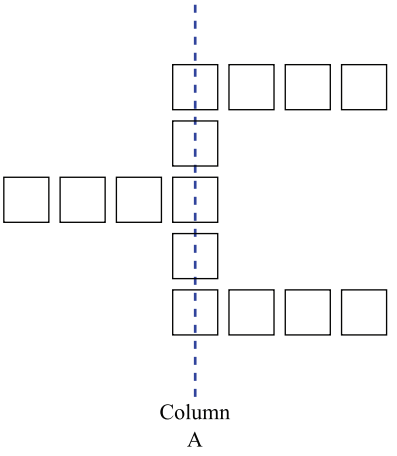

Fig. 16. A fan-out circuit receives a right-ward propagating bit packet and fans it out into two identical packets.

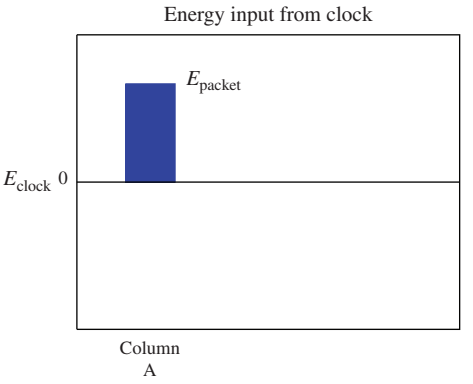

Fig. 17. The energy input from the clock to the cells identified with "Column A" (Fig. 16) is summed over one clock period. The additional energy required to fan a bit packet out into two identical bit packets is the cost of the original packet.

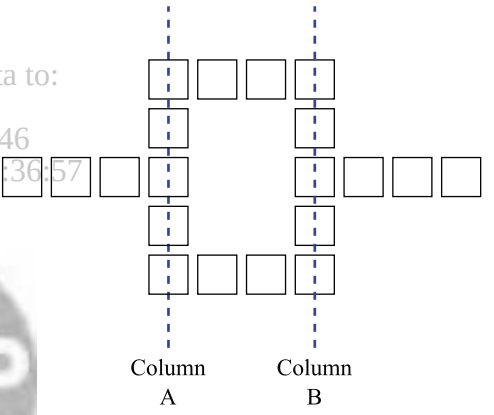

Fig. 18. A fanout circuit receives a right-ward propagating bit packet and fans it out into two identical packets, and then the two packets are combined into one.

The cost of fanning a packet out into multiple copies is the cost of one packet times the number of copies produced. A three-level fanout circuit (depicted in Fig. 20) produces seven bit-packet copies, and clock input over the

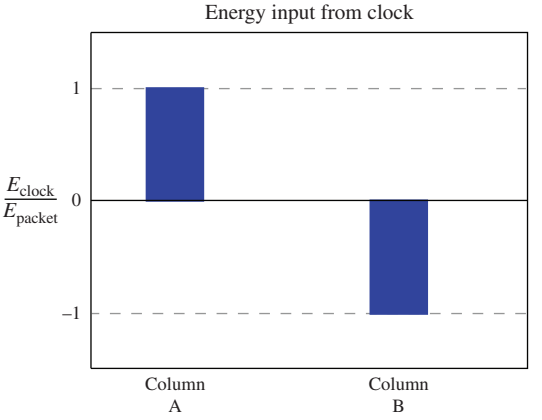

Fig. 19. The energy input from the clock over one clock period required to fan a bit packet out into two is the cost of the original packet, but an equal amount of work is done on the clock when the two bit packets are fanned in to one (fan-in) in column B (Fig. 18).

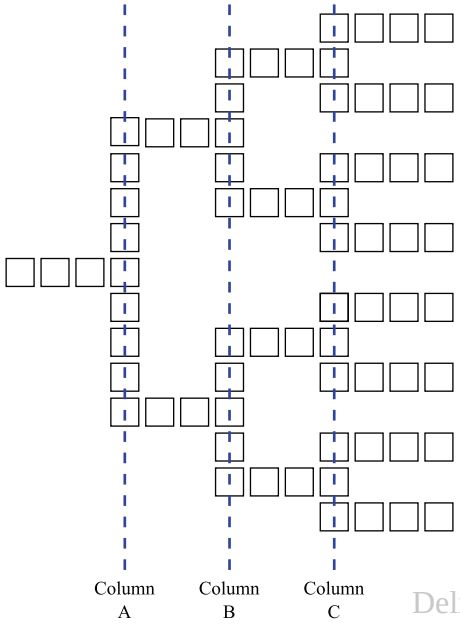

Fig. 20. A three-level fan-out circuit receives a right-ward propagating bit packet and fans it out into eight identical packets.

fanout circuit is seven times the cost of the original packet (Fig. 21).

These results are verified in a dynamic simulation of the fanout circuits[46] in which energy input into the cells is monitored and reported over one full clock period (the dynamic simulation reported in[46] did not include interactions with null cells).

5. ENERGETICS OF BIT PACKETS IN WIDE WIRES

QCA circuits can be designed for robustness by using multiple QCA cells to widen binary wires and QCA devices.[46]

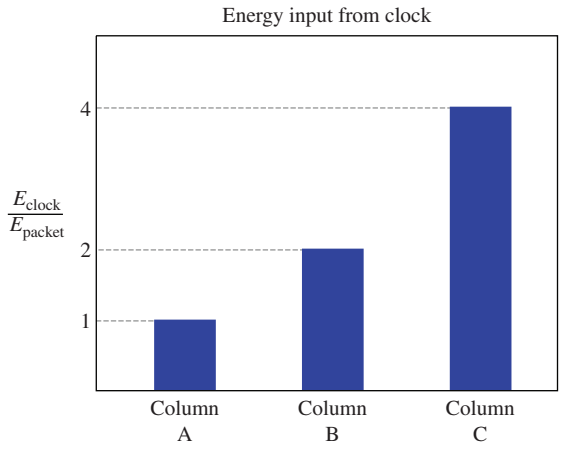

Fig. 21. The energy input from the clock over one period required to fan a bit packet out into eight bit packets is the sum of work done on columns A, B, and C (Fig. 20). The total work done by the clock is seven times the cost of the original packet.

This concept takes advantage of vertical broadside coupling in addition to horizontal broadside coupling.

Consider a bit packet that is N cells long and spans the width of a binary wire R-cells wide as in Figure 22. In addition to the change in energy levels due to horizontal broadside coupling, vertical broadside interactions and a variety of next-nearest-neighbor diagonal interactions must be considered. The energy E_{ref} of a wire of length L and width R with all cells in the null state is

$$E_{ref} = -LRE_{c0} + (L-1)RE_{hnn} + L(R-1)E_{vnn} + 2(R-1)(L-1)E_{dnn} \quad (11)$$

In activating the first column of R cells spanning the width of the wire the following interactions are removed: $2R$ horizontal null-null interactions with energy E_{hnn}; $4(R-1)$ diagonal null-null interactions having energy E_{dnn}; and $R-1$ vertical broadside null-null interactions of energy E_{vnn}. This comes at the cost of RE_{c0} with $R-1$ vertical interactions having energy E_v and $2R$ interactions having energy E_{hn1}, and $2(R-1)$ diagonal interactions between a null cell and a polarized cell having energies E_{dn1} and E_{dn2}. Thus, the first column of cells costs

$$E = RE_{c0} + 2RE_{hn1} + (R-1)E_v + 2(R-1)[E_{dn1} + E_{dn2}] - 2RE_{hnn} - (R-1)E_{vnn} - 4(R-1)E_{dnn} \quad (12)$$

Each additional column of cells costs another $RE_{c0} + (R-1)E_v + (R-1)[E_{dn1} + E_{dn2}]$ and introduces horizontal interactions costing RE_h; it also yields a savings of $RE_{hnn} + (R-1)E_{vnn} + 2(R-1)E_{dnn} + (R-1)[E_{dn1} + E_{dn2}]$. There are $N-1$ additional columns so that the total cost of the R-by-N bit packet in the interior of an R-by-L wire is

$$E = NRE_{c0} + (N-1)RE_h + N(R-1)E_v + (N-1)(R-1)[E_{d1} + E_{d2}]\cdots + 2RE_{hn1} + 2(R-1)[E_{dn1} + E_{dn2}]\cdots - (N+1)RE_{hnn} - N(R-1)E_{vnn} - 2(N+1)(R-1)E_{dnn} \quad (13)$$

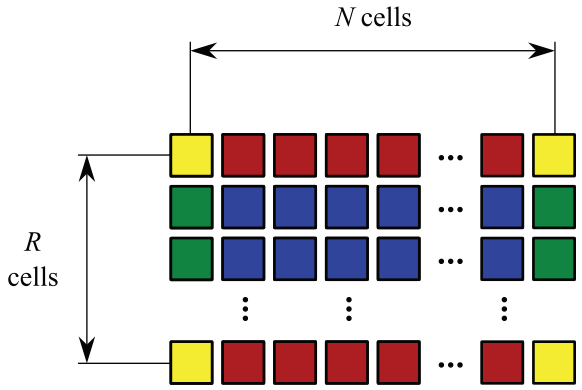

Fig. 22. A bit packet packet of data N cells long and R cells wide. Cells are color-coded to identify different groups of cells. Corner cells are shown in yellow. Skin cells comprise the outer border of the packet. The horizontally-oriented skin is identified in red, and the vertically oriented skin is in green. Bulk cells are color-coded blue.

This cost may also be understood in terms of activating cells of different groups and written in the form

$$E = X_{\text{corner}}E_{\text{corner}} + X_{\text{skin, h}}E_{\text{skin, h}} + X_{\text{skin, v}}E_{\text{skin, v}} + X_{\text{bulk}}E_{\text{bulk}} \tag{14}$$

where X_{corner}, $X_{\text{skin, h}}$, $X_{\text{skin, v}}$, and X_{bulk}, respectively, are the number of cells at the corner of the packet, the number of cells forming the horizontal edges of the packet (not counting the corner cells), the number of cells forming the vertical edges of the packet (not counting the corner cells), and the number of cells internal to the packet; and, E_{corner}, $E_{\text{skin, h}}$, $E_{\text{skin, v}}$, and E_{bulk}, respectively, are the per-cell energy costs associated with each group. The per-cell activation cost for each group are as follows:

$$E_{\text{corner}} = E_{\text{c0}} + E_{\text{hn1}} + \frac{1}{2}(E_{\text{h}} + E_{\text{v}} + E_{\text{dn1}} + E_{\text{dn2}}) + \frac{1}{4}(E_{\text{d1}} + E_{\text{d2}}) \cdots - \frac{3}{2}(E_{\text{hnn}} + E_{\text{dnn}}) - \frac{1}{2}E_{\text{vnn}} \tag{15}$$

$$E_{\text{bulk}} = E_{\text{c0}} + E_{\text{h}} + E_{\text{v}} + E_{\text{d1}} + E_{\text{d2}} - E_{\text{hnn}} - E_{\text{vnn}} - 2E_{\text{dnn}} \tag{16}$$

$$E_{\text{skin, h}} = E_{\text{c0}} + E_{\text{h}} + \frac{1}{2}(E_{\text{v}} + E_{\text{d1}} + E_{\text{d2}}) - E_{\text{hnn}} - \frac{1}{2}E_{\text{vnn}} - E_{\text{dnn}} \tag{17}$$

$$E_{\text{skin, v}} = E_{\text{c0}} + E_{\text{v}} + \frac{1}{2}(E_{\text{h}} + E_{\text{d1}} + E_{\text{d2}}) + E_{\text{hn1}} + E_{\text{dn1}} + E_{\text{dn2}} \cdots - \frac{3}{2}E_{\text{hnn}} - E_{\text{vnn}} - 3E_{\text{dnn}} \tag{18}$$

The number of cells in each group is given by

$$X_{\text{corner}} = 4 \tag{19}$$

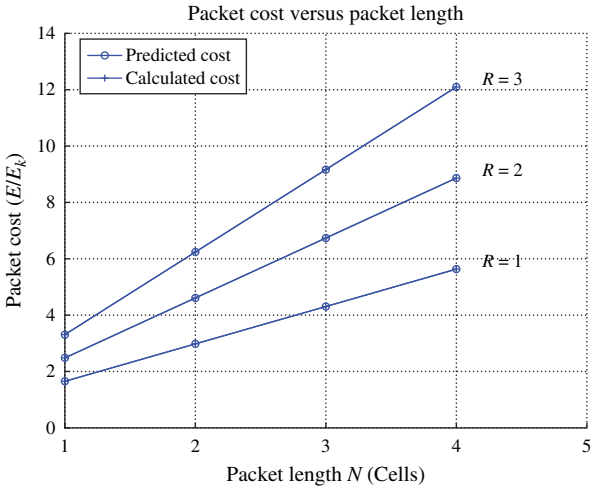

Fig. 23. The cost of a multi-row packet as predicted by the heuristic model using Equations (14)-(22) and calculated from the direct Coulomb model, for various values of packet width R.

$$X_{\text{skin, h}} = 2(N-2) \tag{20}$$

$$X_{\text{skin, v}} = 2(R-2) \tag{21}$$

$$X_{\text{bulk}} = (N-2)(R-2) \tag{22}$$

Equations (14)–(22) are valid when both $R > 2$ and $N > 2$. Figure 23 shows that Eq. (13) [or, equivalently, Eqs. (14)–(22) when valid] accurately predict the cost of a multi-row packet. For these predictions and calculations, cells had $(a, x_{\text{null}}, z_{\text{act}}) = (0.7, 0.175, 0.0875)$ nm; and one positive elementary half-charge is located at each active dot. A center-to-center spacing of 1.4 nm was used for adjacent cells having horizontal or vertical broadside coupling. The clock bias V_{c0} was set such that $E_{\text{c0}} = -E_k$.

6. ENERGY DISSIPATION

The energy cost we are considering here is the energy that must be supplied by the clock to create a QCA bit packet. This energy can be considered "invested" in the QCA signal, but it need not be lost to the environment. As long as the clocking period is long enough for the individual cells to be always near their instantaneous ground state, the condition known as adiabatic clocking, the energy invested in a bit packet is in principle recoverable, i.e., it can be returned to the clocking circuit rather than being dissipated as heat. For molecular systems where the intrinsic switching time is the time it takes for an electron to move from one molecular orbital to another, adiabaticity can be maintained at very high clock rates indeed.

In a real physical system, of course, some energy is always lost to irreversible processes (molecular vibrons, substrate phonons or plasmons, for example). In addition if a logically irreversible calculation is performed there must be dissipation of at least $k_B \ln(2)$ in accordance with Landauer's Principle. These considerations and how to minimize dissipation in practical systems have been discussed elsewhere,[47] though it should be noted that Landauer's Principle itself remains somewhat controversial.[48–53]

7. CONCLUSIONS

Computation with QCA cells instead of transistors requires developing new concepts and abstractions. Conceiving computation as essentially the motion and interaction of bit packets is a helpful abstraction, one level higher than individual QCA cell switching. The energetics of such packets is important because, after all, it is the disastrously high energy dissipation (per unit area) of transistors, that prevents them from being useful in large arrays when simply scaled to molecular dimensions. We have analyzed the energy investment that must be made to create a bit packet. In most instances, the energy required scales with the length of the packet, though we found that one could design length-independent cells (whether such a design

is realizable using synthetic chemistry is another matter). A heuristic model built from just cell-cell interaction energies works very well. Fan-out and fan-in can be simply understood as borrowing or returning bit packed energy to the clocking circuit. We have focused here on the signal energy and not the energy dissipated due to residual non-adiabaticity or bit erasure.

APPENDIX A: THE THREE-STATE APPROXIMATION AND COHERENCE VECTOR FORMALISM

The Three-State Approximation

A three-state model uses three basis vectors $\{|\phi_{-1}\rangle, |\phi_{+1}\rangle, |\phi_{+1}\rangle\}$, each corresponding to one of the active states $[(P, A) = (\mp 1, 1)]$ or the null state $[(P, A) = (0, 0)]$.

In an array of cells, the Hamiltonian $\boldsymbol{H}$ for the jth cell is given

$$\boldsymbol{H}_j = \begin{pmatrix} E_{-1} & 0 & -\gamma \\ 0 & E_{+1} & -\gamma \\ -\gamma & -\gamma & E_{\text{null}} \end{pmatrix} \tag{A1}$$

where each of the diagonal energies include the electrostatic assembly energy of the cell, intercellular interactions, and the applied clock. These matrix elements can be obtained from microscopic models of, for example, the molecular orbitals of a QCA molecule.[35]

7.1. Coherence Vector Formalism

The elements λ_i of the coherence vector $\boldsymbol{\lambda}$ for a cell are the projections of the cell's density matrix $\boldsymbol{\rho}$ onto the generators of SU(3):[54]

$$\lambda_i = \text{Tr}(\boldsymbol{\rho}\boldsymbol{\lambda}_i) \tag{A2}$$

$\boldsymbol{\lambda}_i$ represents the the ith generator of SU(3) as given below.

$$\boldsymbol{\lambda}_1 = \begin{pmatrix} 0 & 1 & 0 \\ 1 & 0 & 0 \\ 0 & 0 & 0 \end{pmatrix} \quad \boldsymbol{\lambda}_2 = \begin{pmatrix} 0 & 0 & 1 \\ 0 & 0 & 0 \\ 1 & 0 & 0 \end{pmatrix}$$

$$\boldsymbol{\lambda}_3 = \begin{pmatrix} 0 & 0 & 0 \\ 0 & 0 & 1 \\ 0 & 1 & 0 \end{pmatrix} \quad \boldsymbol{\lambda}_4 = \begin{pmatrix} 0 & i & 0 \\ -i & 0 & 0 \\ 0 & 0 & 0 \end{pmatrix}$$

$$\boldsymbol{\lambda}_5 = \begin{pmatrix} 0 & 0 & i \\ 0 & 0 & 0 \\ -i & 0 & 0 \end{pmatrix} \quad \boldsymbol{\lambda}_6 = \begin{pmatrix} 0 & 0 & 0 \\ 0 & 0 & i \\ 0 & -i & 0 \end{pmatrix}$$

$$\boldsymbol{\lambda}_7 = \begin{pmatrix} -1 & 0 & 0 \\ 0 & 1 & 0 \\ 0 & 0 & 0 \end{pmatrix} \quad \boldsymbol{\lambda}_8 = \frac{1}{\sqrt{3}} \begin{pmatrix} -1 & 0 & 0 \\ 0 & -1 & 0 \\ 0 & 0 & 2 \end{pmatrix}$$

This is useful because the time evolution of the systems can be expressed in terms of the 8 real degrees of freedom contained in the components of $\boldsymbol{\lambda}$.[46]

References

1. C. Lent, P. Tougaw, and W. Porod, *Appl. Phys. Lett.* 62, 714 **(1993)**.
2. C. Lent, P. Tougaw, W. Porod, and G. Bernstein, *Nanotechnology* 4, 49 **(1993)**.
3. C. Lent and P. Tougaw, *Proc. of the IEEE* 85, 541 **(1997)**.
4. K. Hennessy and C. Lent, *J. Vac. Sci. Technol* 19, 1752 **(2001)**.
5. E. Blair and C. Lent, An architecture for molecular computing using quantum-dot cellular automata, *IEEE C Nanotechnol.*, IEEE **(2003)**, Vol. 1, pp. 402–405.
6. A. O. Orlov, I. Amlani, G. H. Bernstein, C. S. Lent, and G. L. Snider, *Science* 277, 928 **(1997)**.
7. I. Amlani, A. O. Orlov, G. L. Snider, C. S. Lent, and G. H. Bernstein, *Appl. Phys. Lett.* 72, 2179 **(1998)**.
8. G. L. Snider, A. O. Orlov, I. Amlani, G. H. Bernstein, C. S. Lent, J. L. Merz, and W. Porod, *Semiconductor Science and Technology* 13, A130 **(1998)**.
9. G. L. Snider, A. O. Orlov, I. Amlani, G. H. Bernstein, C. S. Lent, J. L. Merz, and W. Porod, *Japanese Journal of Applied Physics Part 1-Regular Papers Short Notes & Review Papers* 38, 7227 **(1999)**.
10. G. L. Snider, A. O. Orlov, I. Amlani, X. Zuo, G. H. Bernstein, C. S. Lent, J. L. Merz, and W. Porod, *J. Appl. Phys.* 85, 4283 **(1999)**.
11. G. L. Snider, A. O. Orlov, I. Amlani, G. H. Bernstein, C. S. Lent, J. L. Merz, and W. Porod, *Microelectronic Engineering* 47, 261 **(1999)**.
12. G. L. Snider, A. O. Orlov, I. Amlani, X. Zuo, G. H. Bernstein, C. S. Lent, J. L. Merz, and W. Porod, *Journal of Vacuum Science & Technology A-vacuum Surfaces and Films* 17, 1394 **(1999)**.
13. I. Amlani, A. O. Orlov, G. L. Snider, C. S. Lent, W. Porod, and G. H. Bernstein, *Superlattices and Microstructures* 25, 273 **(1999)**.
14. I. Amlani, A. O. Orlov, G. Toth, G. H. Bernstein, C. S. Lent, and G. L. Snider, *Science* 284, 289 **(1999)**.
15. A. O. Orlov, I. Amlani, G. Toth, C. S. Lent, G. H. Bernstein, and G. L. Snider, *Appl. Phys. Lett.* 74, 2875 **(1999)**.
16. A. O. Orlov, I. Amlani, R. K. Kummamuru, R. Ramasubramaniam, G. Toth, C. S. Lent, G. H. Bernstein, and G. L. Snider, *Appl. Phys. Lett.* 77, 295 **(2000)**.
17. I. Amlani, A. O. Orlov, R. K. Kummamuru, G. H. Bernstein, C. S. Lent, and G. L. Snider, *Appl. Phys. Lett.* 77, 738 **(2000)**.
18. A. O. Orlov, R. K. Kummamuru, R. Ramasubramaniam, G. Toth, C. S. Lent, G. H. Bernstein, and G. L. Snider, *Appl. Phys. Lett.* 78, 1625 **(2001)**.
19. M. Niemier and P. Kogge, Exploring and exploiting wire-level pipelining in emerging technologies, *28Th Annual International Symposium on Computer Architecture, Proceedings*, ACM Sigarch Computer Architecture News, Gothenburg, Sweden, June **(2001)**, pp. 166–177.
20. A. O. Orlov, R. Kummamuru, R. Ramasubramaniam, C. S. Lent, G. H. Bernstein, and G. L. Snider, *J. Nanosci. Nanotechnol.* 2, 351 **(2002)**.
21. A. O. Orlov, I. Amlani, R. K. Kummamuru, R. Ramasubramaniam, G. Toth, C. S. Lent, G. H. Bernstein, and G. L. Snider, *Appl. Phys. Lett.* 77, 295 **(2000)**.
22. R. K. Kummamuru, A. O. Orlov, R. Ramasubramaniam, C. S. Lent, G. H. Bernstein, and G. L. Snider, *International Electron Devices 2002 Meeting*, Technical Digest **(2002)**, p. 95.
23. A. O. Orlov, R. Kummamuru, R. Ramasubramaniam, C. S. Lent, G. H. Bernstein, and G. L. Snider, *Surface Science* 532, 1193 **(2003)**.
24. R. K. Kummamuru, A. O. Orlov, R. Ramasubramaniam, C. S. Lent, G. H. Bernstein, and G. L. Snider, *IEEE Transactions on Electron Devices* 50, 1906 **(2003)**.

25. R. K. Kummamuru, J. Timler, G. Toth, C. S. Lent, R. Ramasubramaniam, A. O. Orlov, G. H. Bernstein, and G. L. Snider, *Appl. Phys. Lett.* 81, 1332 **(2002)**.
26. K. K. Yadavalli, A. O. Orlov, J. P. Timler, C. S. Lent, and G. L. Snider, *Nanotechnology* 18, 375401 **(2007)**.
27. M. Mitic, M. C. Cassidy, K. D. Petersson, R. P. Starrett, E. Gauja, R. Brenner, R. G. Clark, A. S. Dzurak, C. Yang, and D. N. Jamieson, *Appl. Phys. Lett.* 89, 013503 **(2006)**.
28. S. J. Chorley, C. G. Smith, F. Perez-Martinez, J. Prance, P. Atkinson, D. A. Ritchie, and G. A. C. Jones, *Microelectronics Journal* 39, 674 **(2008)**; *6th International Conference on Low Dimensional Structures and Devices (LDSD 2007)*, San Andres, Colombia **(2007)**.
29. R. P. Cowburn and M. E. Welland, *Science* 287, 1466 **(2000)**.
30. A. Imre, G. Csaba, L. Ji, A. Orlov, G. H. Bernstein, and W. Porod, *Science* 311, 205 **(2006)**.
31. M. B. Haider, J. L. Pitters, G. A. DiLabio, L. Livadaru, J. Y. Mutus, and R. A. Wolkow, *Phys. Rev. Lett.* 102, 046805 **(2009)**.
32. C. S. Lent, *Science* 288, 1597 **(2000)**.
33. H. Qi, S. Sharma, Z. Li, G. L. Snider, A. O. Orlov, C. S. Lent, and T. P. Fehlner, *J. Am. Chem. Soc.* 125, 15250 **(2003)**.
34. H. Qi, Z. H. Li, G. L. Snider, C. S. Lent, and T. P. Fehlner, *Abstracts of Papers of the American Chemical Society* 226, 101 **(2003)**.
35. Y. H. Lu, M. Liu, and C. Lent, *J. Appl. Phys.* 102, 034311 **(2007)**.
36. C. Lent and B. Isaksen, *IEEE T. Electron Dev.* 50, 1890 **(2003)**.
37. Y. H. Lu and C. S. Lent, *Nanotechnology* 19, 155703 **(2008)**.
38. P. Tougaw and C. Lent, *J. Appl. Phys.* 75, 1818 **(1994)**.
39. C. Lent and P. Tougaw, *J. Appl. Phys.* 74, 6227 **(1993)**.
40. J. Timler and C. Lent, *J. Appl. Phys.* 91, 823 **(2002)**.
41. M. Niemier and P. M. Kogge, *Int. Conf. Elec., Circ. Sys.* 1211 **(1999)**.
42. A. O. Orlov, R. Kummamuru, R. Ramasubramaniam, C. S. Lent, G. H. Bernstein, and G. L. Snider, *J. Nanosci. Nanotechnol.* 2, 351 **(2002)**.
43. J. Timler and C. Lent, *J. Appl. Phys.* 94, 1050 **(2003)**.
44. M. Lieberman, S. Chellamma, B. Varughese, Y. Wang, C. Lent, G. H. Bernstein, G. Snider, and F. C. Peiris, *Ann. N. Y. Acad. Sci.* 960, 225 **(2002)**.
45. C. Lent, B. Isaksen, and M. Lieberman, *J. Am. Chem. Soc.* 125, 1056 **(2003)**.
46. M. Liu, Robustness and power dissipation in quantum-dot cellular automata, Ph.D. Thesis, U. of Notre Dame **(2006)**.
47. C. S. Lent, M. Liu, and Y. H. Lu, *Nanotechnology* 17, 4240 **(2006)**.
48. H. Leff and A. Rex, Maxwell's Demon 2: Entropy, Classical and Quantum Information, Computing, Taylor and Francis, London **(2002)**.
49. V. V. Zhirnov, R. K. Cavin, J. A. Hutchby, and G. I. Bourianoff, *Proceedings of the IEEE* 91, 1934 **(2003)**.
50. V. V. Zhirnov and R. K. Cavin, *Nanotechnology* 18, 298001 **(2007)**.
51. R. K. Cavin, V. V. Zhirnov, J. A. Hutchby, and G. I. Bourianoff, *Fluctuations and Noise in Photonics and Quantum Optics III* 5846, IX **(2005)**.
52. J. Earman and J. D. Norton, *Studies In History and Philosophy of Modern Physics* 30B, 1 **(1999)**.
53. J. D. Norton, *Studies In History and Philosophy of Modern Physics* 36B, 375 **(2005)**.
54. G. Mahler and V. A. Weberruss, Quantum Networks: Dynamics of Open Nanostructures, Springer, New York **(1995)**.

Received: 3 April 2010. Accepted: 8 May 2010.